Biomacromolecules

pubs.acs.org/Biomac

Article

Virus-Like Particles as Positive Controls for COVID-19 RT-LAMP Diagnostic Assays

Soo Khim Chan, Pinyi Du, Caroline Ignacio, Sanjay Mehta, Isabel G. Newton, and Nicole F. Steinmetz*

Cite This: *Biomacromolecules* 2021, 22, 1231−1243

Read Online

ACCESS | Metrics & More | Article Recommendations | Supporting Information

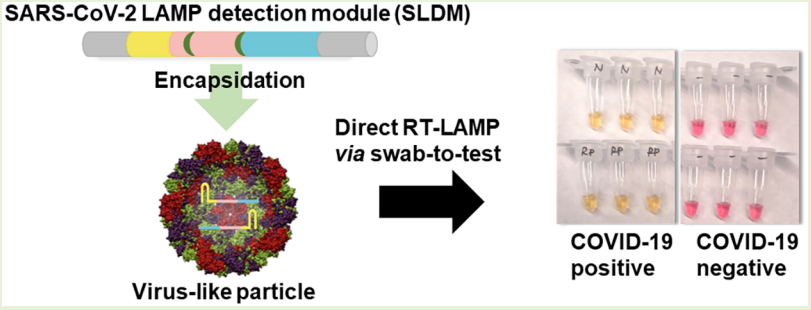

ABSTRACT: Reverse transcription loop-mediated isothermal amplification (RT-LAMP) is a rapid and inexpensive isothermal alternative to the current gold standard reverse transcription quantitative polymerase chain reaction (RT-qPCR) for the detection of severe acute respiratory syndrome coronavirus 2 (SARS-CoV-2). However, unlike RT-qPCR, there are no consensus detection regions or optimal RT-LAMP methods, and most protocols do not include internal controls to ensure reliability. Naked RNAs, plasmids, or even RNA from infectious COVID-19 patients have been used as external positive controls for RT-LAMP assays, but such reagents lack the stability required for full-process control. To overcome the lack of proper internal and external positive controls and the instability of the detection RNA, we developed virus-like particles (VLPs) using bacteriophage Qβ and plant virus cowpea chlorotic mottle virus (CCMV) for the encapsidation of target RNA, namely a so-called SARS-CoV-2 LAMP detection module (SLDM). The target RNA is a truncated segment of the SARS-CoV-2 nucleocapsid (N) gene and human RNase P gene (internal control) as positive controls for RT-qPCR and RT-LAMP. Target RNAs stably encapsidated in Qβ and CCMV VLPs were previously shown to function as full-process controls in RT-qPCR assays, and here we show that SLDMs can fulfill the same function for RT-LAMP and swab-to-test (direct RT-LAMP with heat lysis) assays. The SLDM was validated in a clinical setting, highlighting the promise of VLPs as positive controls for molecular assays.

INTRODUCTION

Severe acute respiratory syndrome coronavirus 2 (SARS-CoV-2) is a betacoronavirus responsible for the COVID-19 pandemic that has led to nearly 1.5 million deaths since the outbreak began in December 2019.[1] Although promising COVID-19 vaccines are due for imminent release, control of the virus will continue to rely on the identification and containment of infected individuals, which requires accurate and widely available COVID-19 tests.[2]

Three types of commercial COVID-19 tests are currently available: molecular diagnostic tests, antigen diagnostic tests, and antibody tests.[3] The current gold standard for the early detection of SARS-CoV-2 infections are highly specific and sensitive molecular tests based on reverse transcription polymerase chain reaction (RT-PCR).[4] However, RT-PCR requires sophisticated instruments, and the turnaround time is typically 1−2 h.[5] A severe global shortage of reagents in the face of unprecedented demand has hampered such testing.[6] Alternatives have been proposed, including the isothermal detection of target RNA[7,8] and variants of the genome-editing tool CRISPR/Cas9 for sequence detection.[9] These tests are suitable for deployment in low-resource settings and can be applied widely as rapid diagnostic tests for diverse populations, particularly those with socioeconomic disadvantages.[10]

Loop-mediated isothermal amplification (LAMP) can detect SARS-CoV-2 RNA in a simple assay that does not require sophisticated equipment and has recently been granted emergency use authorization by the Food and Drug Administration (FDA).[8−11] LAMP allows amplification at a constant temperature and typically has a turnaround time of less than 1 h, which offers improved screening throughput during a pandemic.[12] A combination of reverse transcription

Received: December 7, 2020
Revised: January 21, 2021
Published: February 4, 2021

https://dx.doi.org/10.1021/acs.biomac.0c01727
Biomacromolecules 2021, 22, 1231−1243

and LAMP (RT-LAMP) can detect RNA samples by producing complementary DNA (cDNA) for amplification. RT-LAMP has already been used to detect influenza virus,[13] Ebola virus,[14] and Zika virus.[15] RT-LAMP amplification products can be detected by colorimetry,[13] turbidimetry,[16] fluorescence analysis,[17] or gel electrophoresis.[18] RT-LAMP assays can be carried out anywhere—even in the field, as long as a heat source is available. While the RT-LAMP method is a powerful tool for low-tech and rapid diagnostic testing, the development of the assay is cumbersome due to its complexity: the procedure requires four or six primers that achieve the autocycling strand displacement of oligonucleotides for amplification.[19] LAMP primers, especially the inner primers, require high-performance liquid chromatography (HPLC) purification to reduce nonspecific laddering on agarose gels (which is often used as secondary validation).[20] Another limitation is that multiplex RT-LAMP for simultaneous detection of multiple targets remains challenging due to the complexity of the primer design and challenges to differentiate multiple amplicons. However, newer approaches such as the use of modified primers coupled with biotin tags or fluorophores enable different modes of detection for amplicon subsets using lateral-flow[21] or fluorescent methods[22] and thus hold promise to pave the way for multiplex RT-LAMP detection assays.

Unlike standard quantitative RT-PCR (RT-qPCR) methods, consensus detection regions for RT-LAMP assays have not been recommended by The Centers for Disease Control and Prevention (CDC). Positive controls are therefore tailored according to the gene regions used in different RT-LAMP assays, making this a commercially nonprofitable approach. Internal and external positive controls are used in PCRs to identify false negatives.[23] However, internal positive controls are usually omitted from RT-LAMP assays, possibly because a suitable primer/probe set has not been validated or because a suitable housekeeping gene has not been identified. Accordingly, secondary validation methods are needed to confirm RT-LAMP results, such as LAMP sequencing,[24] RT-qPCR,[25] or agarose gel electrophoresis.[18] Without the pairing of RT-qPCR primer/probe sets, validation of the RT-LAMP internal positive control is challenging. The human β-actin gene was found to be unsuitable as an internal control for clinical samples, suggesting other human genes should be tested as internal control candidates for RT-LAMP.[26]

The commercially approved RT-LAMP test for the detection of SARS-CoV-2 includes synthetic RNAs as external positive controls.[7,11,27] However, these controls are inherently unstable and unable to serve as full-process controls throughout the steps of RNA extraction through to DNA amplification. To overcome this issue of instability, we developed virus-like particles (VLPs) based on bacteriophage Qβ and the plant virus cowpea chlorotic mottle virus (CCMV) for the encapsidation of truncated SARS-CoV-2 RNAs to serve as full-process controls for RT-qPCR.[28]

VLPs are naturally occurring nucleic acid carriers that protect their RNA cargo from degradation by RNases.[29,30] VLPs are noninfectious and can be manufactured at high yields through fermentation in microbial culture or molecular farming in plants.[31] VLPs serve as a nanotechnology platform with unique features compared to contemporary approaches that use lipids[32] or polymers[33] for RNA packaging. A key advantage is the natural property of VLPs to package and stabilize RNA, and their high degree of stability avoids the need of cold chain storage or transport. The VLPs mimic the infectious pathogen; the coat proteins protect the RNA cargo, and therefore VLP-based controls can be used as full-process control, *i.e.*, the VLPs can be handled exactly like patient samples.[28] For these reasons, we have chosen VLPs for the development and implementation of RT-LAMP assays with integrated full-process controls.

We describe a SARS-CoV-2 LAMP detection module (SLDM) in which truncated SARS-CoV-2 nucleocapsid (N) and human RNase P (RP) genes are incorporated into Qβ and CCMV VLPs.[28] These detection regions include binding sites for RT-qPCR and RT-LAMP primers, enabling validation of both techniques in parallel. The RP detection region serves as an internal control for both assays. The encapsidation of the SLDM into VLPs was used to produce three alternative positive control reagents: Qβ 1P-C19L, Qβ 2P-C19L, and CCMV-C19L (the difference between the two Qβ-based constructs is whether these are expressed from a single or two-plasmid system, as elaborated below).

The RT-LAMP products were detected in a colorimetric reaction by observing a pH-dependent color change or by measuring the difference in absorbance at 434 and 560 nm. In the presence of target RNA, phenol red in the RT-LAMP reagent changes in color from pink to yellow due to the accumulation of H^+ ions during amplification.[34] Differences between the absorbance at 434 and 560 nm were tabulated as precise values, with a threshold of $\geq$ 0.3 for the positive detection of SARS-CoV-2 RNA.[24] We also confirmed the success of direct RT-LAMP (also known as the "swab-to-test assay") on COVID-19 clinical samples heated to 95 °C for 5 min to release RNA, avoiding the need for a specific RNA extraction step. The released RNAs could be detected by RT-qPCR and swab-to-test assays. The application of these VLPs as external positive controls was therefore validated in a clinical setting, and the designed RP detection region adequately provided internal control binding sites for both RT-LAMP and RT-qPCR.

MATERIALS AND METHODS

Assembly of the SLDM by PCR. The SLDM was constructed by assembly PCR, which was used to join fragments 1, 2, and 3, as shown in Figure S3. All primers and gene fragments were synthesized by Eurofins Genomics (Table S1). Fragment 1 was amplified from our previous SARS-CoV-2 Detection Module[28] using primers Frag 1 Fw and Frag 1 Rv. Both strands of fragment 2 (N1 and N2) were synthesized *de novo*. Fragment 3 was synthesized in three parts (RP 1, RP 2, and RP 3) with overlapping regions of 12−19 bp for assembly PCR using primers Frag 3 Fw and Frag 3 Rv. The final SLDM construct was prepared by mixing 1 μL (10 ng) of each fragment followed by amplification using primers Frag 1 Fw and Frag 3 Rv. Assembly PCR was carried out using Q5 High-Fidelity 2 × Master Mix (New England Biolabs) in a 25 μL of reaction. The reaction was heated to 98 °C for 30 s, followed by 30 cycles of 98 °C for 10 s, 60 °C for 30 s, and 72 °C for 30 s, and a final extension step at 72 °C for 2 min.

Primer Design for RT-LAMP Assays. The RT-LAMP primers were designed according to the FDA-approved Color SARS-CoV-2 LAMP diagnostic assay.[7,8] All primers were synthesized by Eurofins Genomics (Table S1).

Construction of Plasmids Qβ 1P-C19L and Qβ 2P-C19L. For the one-plasmid system, the SLDM was cloned into vector pCDFDuet-Qβ between restriction sites *Not*I and *Nde*I to generate Qβ 1P-C19L (Figure S2). The insert was placed downstream of the Qβ coat protein gene and was deliberately placed out-of-frame to avoid translation of the N region. For the two-plasmid system, the

https://dx.doi.org/10.1021/acs.biomac.0c01727
Biomacromolecules 2021, 22, 1231−1243

SLDM was transferred to plasmid pET-28a(+) between restriction sites *Bgl*II and *Not*I to generate Qβ 2P-C19L (Figure S2). The upstream ribosome binding site was removed to avoid translation of the N region. All clones were verified by Sanger sequencing (Eurofins Genomics).

Production of Qβ 1P-C19L and Qβ 2P-C19L VLPs. The Qβ 1P-C19L and Qβ 2P-C19L plasmids were introduced into *E. coli* BL21 (DE3) competent cells (New England Biolabs) and plated on LB medium containing 100 μg/mL streptomycin (Qβ 1P-C19L) or 100 μg/mL streptomycin plus 50 μg/mL kanamycin (Qβ 2P-C19L). VLPs were expressed and recovered from the cells, as previously described.[28]

Expression of SLDM by *In Vitro* Transcription. The SLDM was amplified using primers Frag 1 Fw and Frag 3 Rv, and the linearized construct was transcribed *in vitro* using the MEGAscript T7 transcription kit (Thermo Fisher Scientific). The SLDM RNA was purified using the MEGAclear transcription clean-up kit (Thermo Fisher Scientific). The concentration and purity of the SLDM RNA were determined by measuring the absorbance ratio at 260/280 and 260/230 nm using a Nanodrop 2000/2000c spectrophotometer (Thermo Fisher Scientific). The integrity of the RNA was confirmed by visualization on a Novex 6% urea TBE gel (Thermo Fisher Scientific).

Production of CCMV-C19L VLPs. CCMV-infected *Vigna unguiculate* leaves were harvested 12 days post-infection (protocols carried out under USDA-approved P526 permits) followed by CCMV purification, as previously described.[35] CCMV coat proteins were obtained by disassembly[36,37] and were reassembled with *in vitro* transcribed SLDM RNA with 6:1 mass ratio.[36] The concentration of reconstituted CCMV was determined using a Pierce BCA protein assay kit (Thermo Fisher Scientific).

Characterization and Validation of VLP-Based SLDM Positive Controls. The VLPs were characterized by transmission electron microscopy (TEM), dynamic light scattering (DLS), agarose gel electrophoresis, and size exclusion chromatography (SEC), as previously reported.[28] For validation as positive controls, SLDM RNA was extracted using the QIAamp Viral RNA Mini Kit (Qiagen) and amplified by RT-qPCR using the SuperScript III Platinum One-step RT-qPCR kit (Thermo Fisher Scientific) on a CFX96 Touch real-time PCR detection system (Bio-Rad). Amplification efficiency in the N region was determined using the N1 primer/probe set 2019-nCoV CDC qPCR Probe Assay (Integrated DNA Technologies, cat. no. 10006713). Amplification efficiency in the RP region was determined using the TaqMan Gene Expression Assay with FAM probes (Applied Biosystems, assay ID Hs01921656_s1). In each case, serially diluted samples contained 10^6–10^0 copies of SLDM RNA. All samples were tested in triplicate. Quantification cycle (C_q) values were tabulated using CFX Maestro Software.

Stability of VLP-Based SLDM Positive Controls. *Incubation at Various Temperatures over Time.* Free SLDM RNAs (5 ng) and VLP-based positive controls (10 μg) were aliquoted to a total volume of 20 μL and stored at five different temperatures (−80 °C, −20 °C, 4 °C, room temperature: 15–20 °C, 40 °C) for 1 day, 3 days, and 1 week, respectively. RNA was extracted from VLPs as mentioned above, and 1 μL of eluted RNA/free SLDM RNA was used in RT-qPCR as mentioned previously using RP primers/probe. All samples were assayed in triplicates on a Bio-Rad CFX96 Touch real-time PCR detection system. Quantification cycle (C_q) values were tabulated by CFX Maestro software.

RNase A Digestion. Free SLDM RNAs (200 ng) and VLP-based positive controls (10 μg) were incubated with 25 μg of RNase A (Thermo Scientific) at 37 °C for 30 min. VLP-based positive controls were purified with Amicon Ultra 0.5 mL centrifugal filter (100 kDa) to remove the RNase A. Purified VLP-based positive controls, with or without (control) RNase digestion (samples not subjected to RNase digestions were also incubated at 37 °C for 30 min to factor in the possibility of RNA degradation over time), were analyzed by agarose gel electrophoresis. Free SLDM RNAs, with or without RNase treatment, were analyzed by Novex TBE-Urea gels (6%; Thermo Fisher Scientific).

RNA Release Kinetics. We incubated 15 μg of VLPs in a total volume of 20 μL for 5 min at 95 °C. The acidic CCMV storage buffer (0.1 M sodium acetate, 1 mM EDTA, pH 4.8) was first replaced with 1× PBS buffer using Amicon Ultra 0.5 mL 100 kDa centrifugal filters to avoid the acidic buffer from triggering false-positive results in the RT-LAMP assay. The concentration of CCMV-C19L in PBS was determined using the Pierce BCA protein assay kit. VLP samples before and after heating were fractionated by agarose gel electrophoresis, and the RNA bands were excised for further analysis.[28] We used 1 μL of the eluted RNA for RT-qPCR and RT-LAMP assays using the N and RP primer/probe sets.

RT-LAMP Assays. RT-LAMP assays were carried out using WarmStart Colorimetric RT-LAMP 2× Master Mix (New England Biolabs). All primers were mixed to make a 10× stock, and the reaction was prepared with 12.5 μL WarmStart Colorimetric RT-LAMP 2× Master Mix, 2.5 μL 10 × primer stock, 1 μL of sample, and topped up to 25 μL with nuclease-free water (Zymo Research). All samples were tested in duplicate. The reaction mix was incubated at 65 °C for 55 min with the heated lid at 105 °C in a PTC-200 Thermal Cycler Dual 48 (MJ Research). The heated reaction mix was cooled to room temperature for 5 min, the color change was photographed, and the absorbance was measured at 434 and 560 nm using an Infinite 200 Rx plate reader (Tecan Life Sciences) with 25 flashes in 96-well V-bottom plate mode. The absorbance color change ($\Delta Abs_{434-560}$) was calculated by subtracting the absorbance at 560 nm from the absorbance 434 nm.

Swab-to-Test Assay. As above, CCMV-C19L was first exchanged into PBS to avoid false positives. We heated 10 μL of the patient samples or positive controls to 95 °C for 5 min in a PCR tube and then transferred the tube immediately to a cooling block at 4 °C. We added 1 μL of sample to 19 μL of RT-LAMP reaction mix (see above) in a hard-shell 96-well PCR plate (Bio-Rad), sealed the plate with a transparent heat seal (Bio-Rad), and incubated at 65 °C for 55 min with the heating lid at 105 °C. The color change was recorded as above. A range of SLDM positive controls (10^0, 10^1, 10^2, 10^3, 10^4, 10^5, and 10^6 copies) was used to investigate the detection limit of the assay and a no template control (NTC) was also included. RNA released from VLPs was also analyzed by RT-qPCR using primer/probe sets for N and RP to determine the cutoff C_q value.

Clinical Validation. For the ddPCR test, 10 μg of VLP samples were extracted using the QIAamp Viral RNA mini kit and eluted in 140 μL of AVE buffer. We diluted 10 μL of the eluted RNA 10^6-fold in RNase-free water. A clinical sample from a COVID-19 patient was used as a positive control, and a sample from a healthy patient was used as a negative control. The samples were diluted 100-fold in RNase-free water. A no template control (NTC) was included to rule out contamination. Each reaction was carried out triplicate using the N and RP primer/probe sets, as previously reported.[28] For the swab-to-test assay, 10 μL of patient samples or positive controls (10^6 copies) were heated at 95 °C for 5 min, and 1 μL of the heated solution was mixed with 19 μL of RT-LAMP reaction mix as described above.

RESULTS AND DISCUSSION

Design of the SARS-CoV-2 SLDM and Its Encapsulation into VLPs. The SLDM was designed with N and RP detection regions consisting of primer/probe binding sites for RT-LAMP and RT-PCR. The N detection region for RT-PCR was based on CDC recommendations (N1), and the RP detection region for RT-PCR was based on the human *POP7* gene encoding RNase P, which is used for RT-LAMP detection. The RT-LAMP detection regions for both genes were designed based on the Color SARS-CoV-2 LAMP Diagnostic Assay,[7] which has been granted emergency use authorization by the FDA. This assay has a detection limit of 0.75 copies of viral RNA per microliter of primary sample and shows 100% agreement with laboratory results for 543 clinical samples; the readout measures differences in absorbance.[7] RT-

https://dx.doi.org/10.1021/acs.biomac.0c01727
Biomacromolecules 2021, 22, 1231−1243

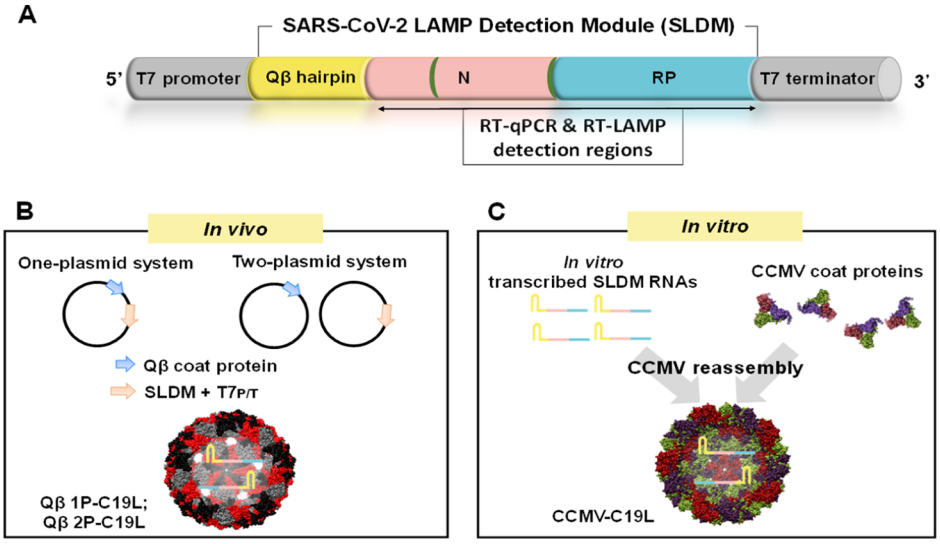

Figure 1. Construction of SLDM positive controls. (A) Design of SLDM from 5′ to 3′: T7 promoter (gray), Qβ hairpin (yellow), N (pink), restriction sites (green), RP (blue), and T7 terminator (gray). The N and RP segments contain both RT-qPCR and RT-LAMP detection regions. (B) Production of Qβ 1P-C19L and Qβ 2P-C19L VLPs *in vivo*. Qβ 1P-C19L: VLPs were produced using a one-plasmid system, in which the SLDM and Qβ coat protein genes were present on the same vector (pCDFDuet-1). Qβ 2P-C19L: VLPs were produced using a two-plasmid system, in which SLDM RNA was produced from pET-28a (+), and Qβ coat protein was produced from pCDFDuet-Qβ. (C) CCMV-C19L VLPs were produced by the reassembly of *in vitro* transcribed SLDM RNAs and purified CCMV coat proteins.

LAMP and RT-PCR should detect the same gene to allow true comparison and validation, and this is achieved in our SLDM by designing both target regions with primer/probe sets for detection by RT-LAMP (assay) and RT-PCR (validation and calculation of SLDM copy number for each positive control).

The 801-nt SLDM sequence is divided into three segments (Figure 1A): a 29-nt Qβ hairpin that links the RNA to Qβ coat proteins during encapsidation,[38] the SARS-CoV-2 N gene (accession NC_045512.2) providing the detection region for both RT-PCR (gene location 28271−28443) and RT-LAMP (gene location 29081−29320), and the RP gene (accession NM_005837.2, gene location 581−930) providing the detection region for both RT-PCR and RT-LAMP. Restriction sites *Pst*1 and *Sal*1 were placed between the sequences to facilitate subcloning, and further restriction sites (Qβ 1P-C19L: *Not*1, *Nde*1; Qβ 2P-C19L: *Not*1) were placed before the T7 promoter and after the T7 terminator (Figures 1A and S1). There is no CDC-defined standard RT-LAMP detection region, and our design allows other detection regions to be inserted in the place of those described (including the internal control detection region).

The T7 promoter and terminator drive transcription, enabling the encapsidation of SLDM RNAs into Qβ and CCMV VLPs *in vivo* and *in vitro*, respectively (Figures 1 and S1). The SLDM cassette flanked by the T7 promoter and terminator (SLDM + $T7_{P/T}$) was transferred to the vectors pCDFDuet-Qβ and pET-28a (+) to generate Qβ 1P-C19L and Qβ 2P-C19L, respectively (Figure S2). The one-plasmid system (Qβ 1P-C19L) allows the co-expression of the Qβ coat protein gene and SLDM RNA from the same vector (Figure S3), whereas the two-plasmid system[29,39] requires the co-transformation of bacteria with plasmids Qβ 2P-C19L and pCDFDuet-Qβ for the encapsidation of SLDM RNA in Qβ VLPs (Figure S3). Qβ VLPs were obtained by expression in *Escherichia coli* (Figure 1B), whereas CCMV-based biomimetic VLPs were obtained by the assembly of purified coat proteins (from CCMV produced in plants) with *in vitro* transcribed SLDM RNA (Figure 1C).

The SLDM + $T7_{P/T}$ cassette was intentionally misaligned with the open reading frame of the plasmid to avoid translation of the truncated SARS-CoV-2 N gene segment. The upstream ribosome binding site was likewise removed, which not only prevents translation but also avoids competition with the Qβ coat protein to bind the target RNA.[29] The upstream ribosome binding site of the Qβ coat protein was retained for protein translation. A *Pst*I restriction site was placed between the RT-PCR and RT-LAMP primer binding sites to further scramble the N gene sequence, as well as provide another accessible cloning site for future adaptations. The SLDM RNAs transcribed *in vitro* were analyzed by electrophoresis in denaturing urea polyacrylamide gels, revealing a size of ∼800 nt, as anticipated (Figure S4A). The presence of functional binding sites in the SLDM RNA was confirmed by both RT-PCR (Figure S4C) and RT-LAMP (Figure S4D).

The rationale for selecting CCMV and Qβ VLPs in this study was to adopt well-established technology (rather to develop novel VLP nanotechnology) and pivot toward COVID-19 applications. Both VLPs can be produced at scale through microbial fermentation or molecular farming. We selected two distinct VLPs: a bacteriophage and plant virus with distinct structure and RNA encapsulation mechanism. Qβ VLPs encapsidate foreign RNAs both *in vivo* by co-expression[39] and *in vitro* by assembly;[40] however, the *in vitro* encapsidation method is relatively complex, requiring multiple processing steps. On the contrary, *in vitro* encapsidation using CCMV VLPs follows a simple and well-established protocol.[41] On the downside when starting from scratch, CCMV VLP production would be delayed due to the need to establish a plant molecular farming assembly line—the first batch of CCMV could be obtained within 1 month starting from seed to purified and assembled CCMV VLP packaging the target RNA. In contrast, the expression of recombinant Qβ VLPs is carried out overnight. Because of the differences, we set out to

https://dx.doi.org/10.1021/acs.biomac.0c01727
Biomacromolecules 2021, 22, 1231−1243

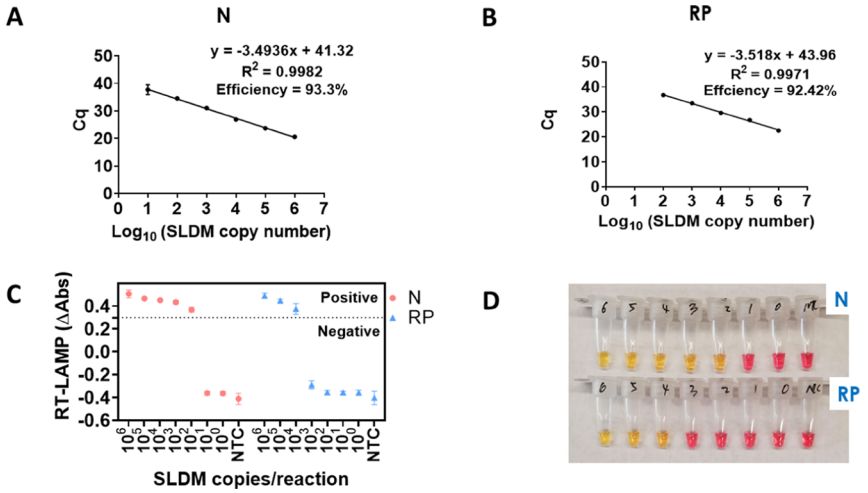

Figure 2. Validation of primer/probe sets using *in vitro* transcribed SLDM RNAs. RT-qPCR was performed on *in vitro* transcribed SLDM RNAs (10^6–10^0 copies) to construct standard curves for the (A) N and (B) RP regions to tabulate PCR amplification efficiency. Error bars show the standard deviation. (C) RT-LAMP was performed on *in vitro* transcribed SLDM RNAs (10^6–10^0 copies) to determine the detection limits for N and RP using RT-LAMP primers. (D) Images of the RT-LAMP reactions were captured following incubation at 65 °C for 55 min to show the color change. A no template control (NTC) was included as a negative control. Numbers on tubes represent powers of 10 in terms of SLDM RNA copies (*e.g.*, 6 = 10^6 copies).

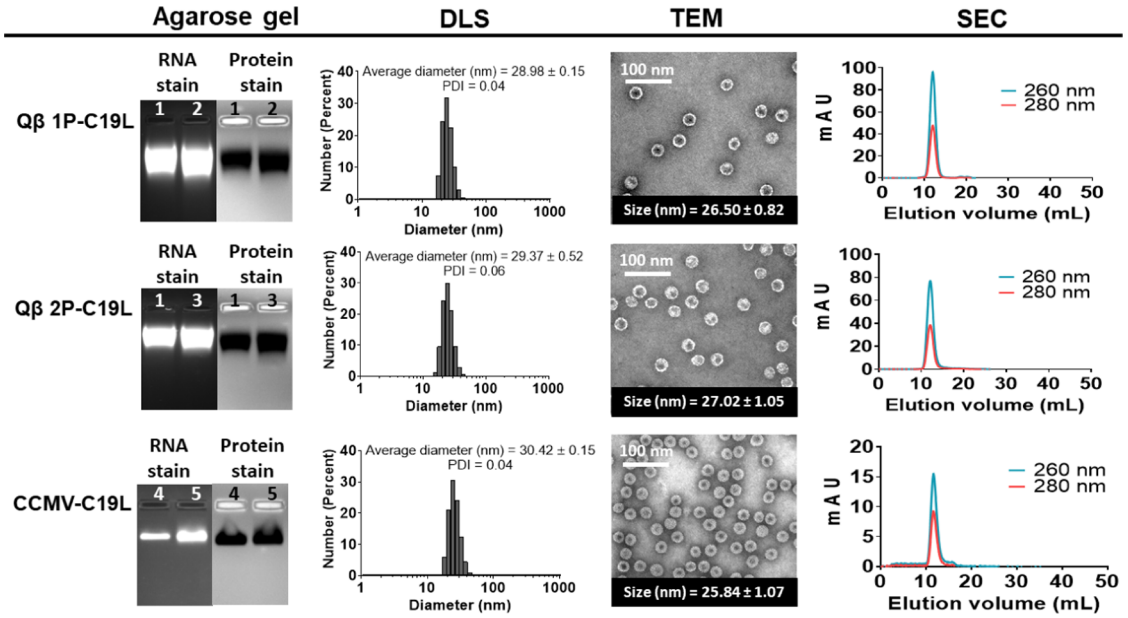

Figure 3. Characterization of VLP-based SLDM positive controls. The first column shows the analysis of VLPs by native agarose gel electrophoresis followed by staining with GelRed (nucleic acid stain) and Coomassie Brilliant Blue (protein stain), confirming that particles are intact: lane 1 = Qβ VLPs; lane 2 = Qβ 1P-C19L; lane 3 = Qβ 2P-C19L; lane 4 = wild-type CCMV; and lane 5 = CCMV-C19L. The second column shows the analysis of VLPs by dynamic light scattering (DLS). Triplicate samples were analyzed, and representative data sets are shown. PDI represents polydispersity index. The third column shows negatively stained VLPs analyzed by transmission electron microscopy (TEM). The average size of 20 particles tabulated by ImageJ software is presented below each image. The final column shows the analysis of VLPs by size exclusion chromatography (SEC) using a Superose 6 column and GE Healthcare Äkta Purifier chromatography system. Nucleic acids were detected at 260 nm, and protein was detected at 280 nm.

study both systems in parallel to provide comprehensive protocols and foundation to develop appropriate positive controls and RT-LAMP assays for COVID-19 diagnostics. Armored RNA technology using bacteriophage MS2 by Asuragen has demonstrated the utility of VLPs as positive controls in molecular diagnostic assays.[42] However, Qβ VLPs outperform MS2 by having higher thermal stability[43] and higher payload capacity.[44] Despite being well studied, CCMV VLPs have not yet been explored as a platform technology in diagnostic assays. An advantage of the CCMV system is that *in vitro* encapsidation yields 100% of the target RNA being packaged; in contrast, target RNA packaged into Qβ VLPs makes only a fraction of the payload because Qβ also packages *E. coli* host RNAs during assembly.[39]

Validation of *In Vitro* Transcribed SLDM RNAs by RT-PCR and RT-LAMP. We validated the amplification efficiency of SLDM RNA by RT-qPCR using serial dilutions of the template. The amplification efficiency was calculated from the

https://dx.doi.org/10.1021/acs.biomac.0c01727
Biomacromolecules 2021, 22, 1231−1243

Table 1. Total Nucleic Acids Extracted from VLP-Based SARS-CoV-2 Positive Controls and the Proportion Represented by SLDM RNA

	Qβ	Qβ 1P-C19L	Qβ 2P-C19L	CCMV-C19L
total nucleic acids (ng/μL)[a]	116.03 ± 6.26	125.83 ± 11.20	124.63 ± 10.62	105.83 ± 19.40
260/280	3.09 ± 0.04	3.08 ± 0.02	3.04 ± 0.05	3.19 ± 0.06
260/230	2.62 ± 0.46	2.28 ± 0.27	2.47 ± 0.50	2.47 ± 0.51
normalized copy number (10^)[b]	n/a	9.39 ± 0.11	8.93 ± 0.06	9.74 ± 0.25
proportion of SDM RNAs in total RNAs (%)	n/a	21.00	7.30	47.00

[a]Total nucleic acids include carrier RNA. [b]Normalized copy number for every 4.5 ng of total nucleic acids was tabulated to obtain the quantity of SLDM RNAs as a proportion of total RNAs.

slope of the standard curve using the equation: $E = (10^{-1/\text{slope}} - 1) \times 100\%$.[45] The N and RP primer/probe sets both achieved an amplification efficiency > 90% with a correlation coefficient (R^2) > 0.99 (Figure 2), matching the ideal efficiency of RT-qPCR.[46] The primer/probe sets were also able to detect as few as 10 copies of N and 100 copies of RP with a C_q < 40. The sensitivity and efficiency of the N primer/probe sets using RNA transcripts or genomic RNA extracted directly from clinical samples have been reported previously.[47,48] The RP primer/probe set used in this study has not previously been used as a control for the detection of SARS-CoV-2 by RT-qPCR, but we confirmed the detection of the human RP gene in clinical samples by droplet digital PCR (ddPCR), as discussed below. Therefore, we concluded that our SLDM RNA construct was suitable as a SARS-CoV-2 positive control for RT-qPCR and for the validation of the RT-LAMP assay proposed herein.

The detection limit of the *in vitro* transcribed SLDM RNA was higher in the RT-LAMP assay than the RT-qPCR, a phenomenon observed in some studies[18,24] but not others.[49,50] The difference in detection limit reflects the use of different sets of primers with different specificities for each assay. As discussed above, the RT-LAMP triggered a color change from pink to yellow in the presence of target RNAs due to the release of H^+ ions from DNA amplification, and we defined a positive result as a difference in absorbance values at 434 and 560 nm of ≥0.3, as previously described.[24] The SLDM detection in RT-LAMP assays was 100 copies using the N primers and 10^4 copies using the RP primers, equivalent to RT-qPCR C_q values of 35 and 30, respectively (Figure 2C,D). The SLDM RNA has a much higher detection limit using primers from Color Genomics, perhaps reflecting differences in the construct as well as the RNA extraction method, final elution volume, and detection method. However, the higher detection limit can be overcome by calculating the quantity of VLPs needed to achieve an SLDM RNA load that provides a sufficient positive control.

Production and Characterization of VLP-Based SLDM Positive Controls. The VLP-based SLDM positive controls were characterized by native agarose gel electrophoresis, dynamic light scattering (DLS), transmission electron microscopy (TEM), and size exclusion chromatography (SEC), as shown in Figure 3. All three VLP formats were intact, monodisperse particles, devoid of free nucleic acids or proteins. Accordingly, the VLPs showed matching band patterns when stained with GelRed (RNA stain) and Coomassie Brilliant Blue (protein stain), confirming the particle intactness. The hydrodynamic size of Qβ 1P-C19L and Qβ 2P-C19L particles was ∼29 nm (polydispersity index = 0.04−0.06) and that of CCMV-C19L particles was ∼30 nm (polydispersity index = 0.04), similar to the corresponding wild-type viruses.[28] TEM images revealed particles slightly smaller than the corresponding DLS measurements due to differences in particle states (dried and stained in TEM *vs* hydrated in DLS) specifically 26−27 nm for Qβ 1P-C19L and Qβ 2P-C19L, and 26 nm for CCMV-C19L, again similar to the wild-type viruses.[28,36] The structural integrity of all particles was confirmed by the concurrent SEC elution profiles of nucleic acid (260 nm) and protein (280 nm) from the Superose 6 column at ∼12 mL, with no additional peaks representing free RNA or protein.[51,52]

RNA was extracted from the VLPs using the QIAamp Viral RNA Mini Kit recommended by the CDC, which includes carrier RNA (assumed to be present at the same concentration for all extracts). The total nucleic acid concentration of Qβ 1P-C19L and Qβ 2P-C19L extracts was higher than that of Qβ VLPs, the difference representing the normalized copy number of SLDM RNAs (Table 1). CCMV-C19L extracts contained the lowest concentration of total nucleic acids but the highest normalized copy number of SLDM RNAs (Table 1). These results agreed with our previous findings.[28] The total nucleic acids extracted from VLPs were highly pure, with 260/230 and 260/280 ratios > 2.

The SLDM copy number was calculated based on the standard curves (Figure 2A,B). CCMV-C19L particles contained the highest SLDM copy number ($10^{9.74}$ copies of SLDM RNA per particle, equivalent to ∼47% of total nucleic acids in the extract) followed by Qβ 1P-C19L ($10^{9.39}$ copies, 21%) and Qβ 2P-C19L ($10^{8.93}$ copies, 7.3%), in agreement with our earlier report.[28] CCMV-C19L was expected to encapsidate the largest quantity of SLDM RNA because the CCMV-C19L particles were assembled with pure *in vitro* transcribed SLDM RNAs, which were subsequently detected in the extracts (Figure S5). In contrast, SLDM RNAs competed with *E. coli* RNA to be encapsidated in the Qβ 1P-C19L and Qβ P2-C19L particles, resulting in a lower SLDM RNA copy number. The higher SLDM copy number in Qβ 1P-C19L compared to Qβ 2P-C19L particles reflected the higher transcription and/or encapsidation efficiency of the one-plasmid system.[28]

To determine the batch-to-batch consistency of VLPs, SLDM RNAs were extracted from three separate batches and the amount of SLDM per VLP was determined by RT-qPCR. CCMV-C19L demonstrated the batch-to-batch consistency with the lowest standard deviation (± 0.20) in the C_q value (Figure S6). This is expected, as the amount of SLDM RNA loaded into each particle has been carefully adjusted to neutralize the basic N-terminus of CCMV coat proteins. Furthermore, only *in vitro* transcribed SLDM RNAs were packaged into CCMV VLPs, leading to lower batch-to-batch variability. While Qβ 1P-C19L and Qβ 2P-C19L also showed batch-to-batch consistency, the larger standard deviation

https://dx.doi.org/10.1021/acs.biomac.0c01727
Biomacromolecules 2021, 22, 1231−1243

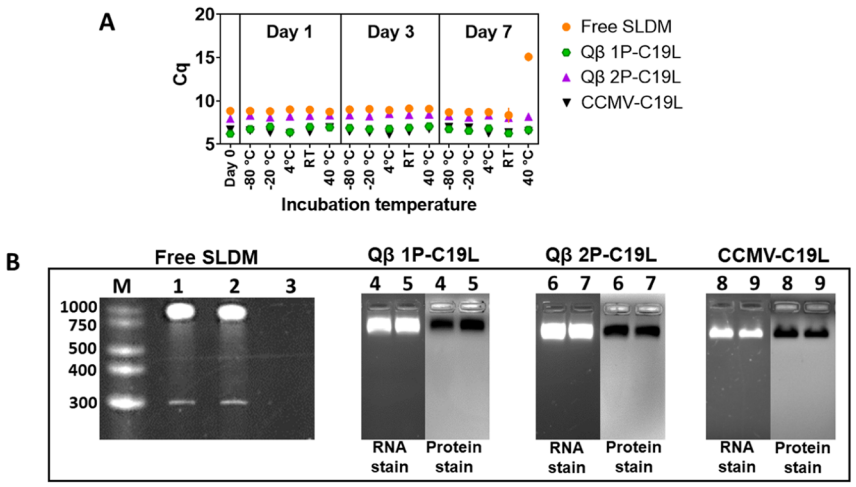

Figure 4. Comparison of stability of free and VLP-encapsidated SLDM RNAs. (A) Temperature/time incubation test. The stability of free SLDM RNAs and VLP-encapsidated SLDM RNAs in respect to time and temperature was plotted against C_q values. Triplicates were performed on each sample with the error bar showing the standard deviation. (B) RNase A digestion test: Free SLDM RNAs were analyzed with denaturing urea polyacrylamide gel, and all VLP-based positive controls were analyzed with native agarose gel electrophoresis. (M) Century-Plus RNA markers. (Lane 1) Fresh free SLDM RNA. (Lane 2) Free SLDM RNA incubated at 37 °C. (Lane 3) Free SLDM RNA incubated at 37 °C with 25 μg RNase A. (Lane 4) Qβ 1P-C19L incubated at 37 °C. (Lane 5) Qβ 1P-C19L incubated at 37 °C with 25 μg RNase A. (Lane 6) Qβ 2P-C19L incubated at 37 °C. (Lane 7) Qβ 2P-C19L incubated at 37 °C with 25 μg RNase A. (Lane 8) CCMV-C19L incubated at 37 °C. (Lane 9) CCMV-C19L incubated at 37 °C with 25 μg RNase A.

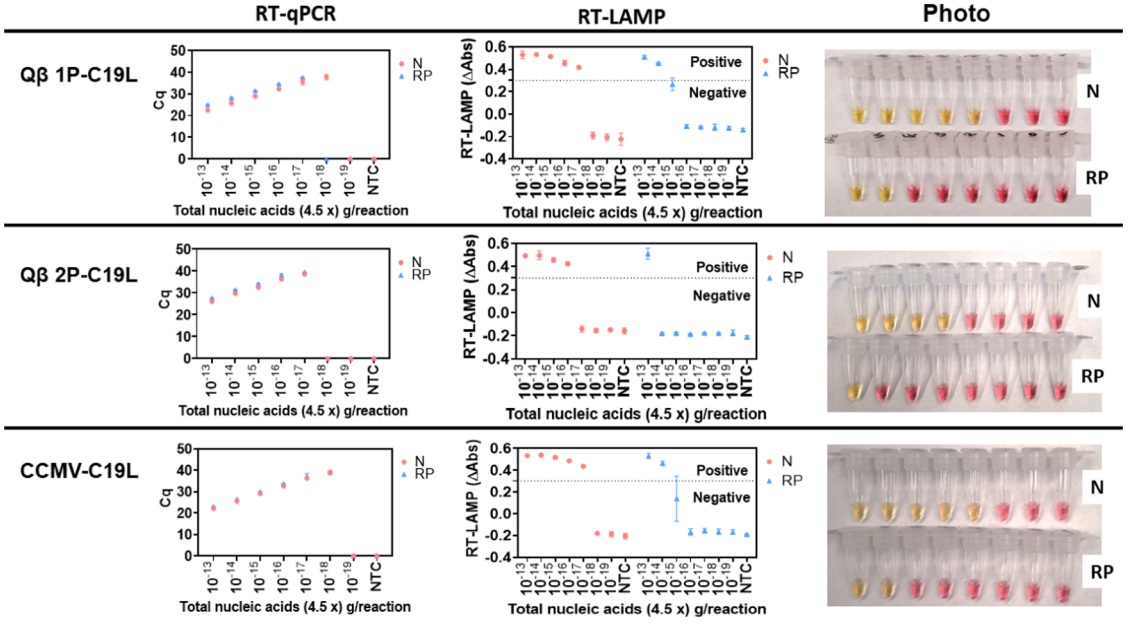

Figure 5. Serial dilutions of total nucleic acids extracted from VLPs analyzed by RT-qPCR and RT-LAMP. The extracts were analyzed to detect the presence of SLDM RNAs. Error bars depict standard deviations. In the RT-LAMP assay, the dotted line at 0.3 on the *y*-axis separates the positive and negative clusters. Images indicate the color change in the RT-LAMP assay and are arranged according to the *x*-axis in the RT-qPCR panel (NTC = no template control).

around 0.3−0.4 in C_q values can be explained by the fact that Qβ VLPs package a mix of target and *E. coli* host RNAs (Figure S6). Statistical analysis using one-way analysis of variance (ANOVA) showed that there was no significant difference comparing the batches of either CCMV-C19L or Qβ 1P-C19L. For the two-plasmid system (Qβ 2P-C19L); however, significant difference (p = 0.02) between the batches was apparent. This observation is in agreement with our previous report[28] and indicates that the two-plasmid system is less reliable. The one-plasmid system and/or CCMV VLP would be the most favorable option for scaled-up manufacture of the proposed positive controls.

Stability of VLP-Based SLDM Positive Controls. Stability of free *vs* VLP packaged SLDM RNAs was assessed using two stability tests: first, free SLDM *vs* VLPs (Qβ 1P-C19L, Qβ 2P-C19L, CCMV-C19L) were incubated at various temperatures (−80 °C, −20 °C, 4 °C, room temperature: 15−20 °C, 40 °C) and stability was measured over time (1 day, 3 days, and 1 week); and second, free SLDM *vs* VLPs (Qβ 1P-C19L, Qβ 2P-C19L, CCMV-C19L) were subjected to RNase

https://dx.doi.org/10.1021/acs.biomac.0c01727
Biomacromolecules 2021, 22, 1231−1243

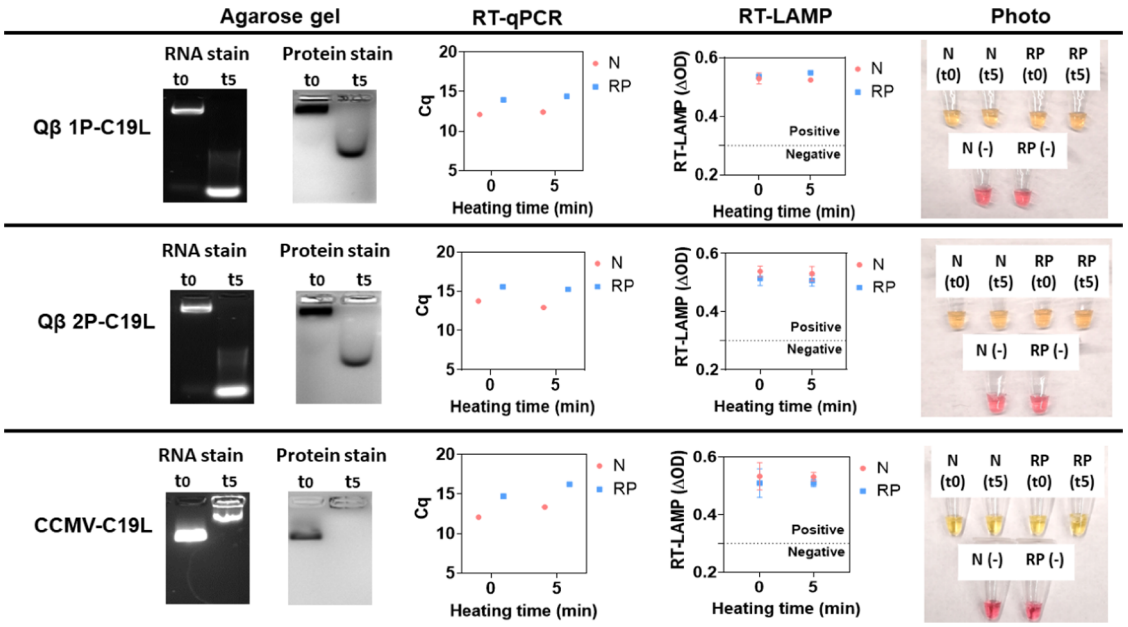

Figure 6. Release of RNA from VLPs. VLPs before heating (t0) and after 5 min at 95 °C (t5) were analyzed by native agarose gel electrophoresis. The RNA and protein in the gels were stained with GelRed and Coomassie Brilliant Blue, respectively. The RNA bands were excised and analyzed by RT-qPCR and RT-LAMP to confirm the presence of SLDM RNAs. Error bars depict standard deviations. In the RT−LAMP assay, the dotted line at 0.3 on the *y*-axis separates the positive and negative clusters. Images indicate the color change in the RT-LAMP assay, with N(−) and RP(−) representing the no template control.

A digestion. For longitudinal stability assays, conditions were chosen to mimic temperature ranges experienced during shipping and storage. Approximately 98% of free SLDM RNA was degraded when incubated for 1 week at 40 °C (Figure 4A; significant reduction in the C_q value from 8.85 ± 0.15 at day 0 to 15.08 ± 0.53 at day 7); however, no significant degradation was observed for other conditions tested (with C_q values remaining consistent around 8.86 ± 0.20). In contrast, all three positive controls (Qβ 1P-C19L, Qβ 2P-C19L, CCMV-C19L) remained stable during any condition and over the 1 week time course (with a standard deviation of C_q values around ± 0.16 to ± 0.26). The small range in C_q values is most likely explained by pipetting and other handling inconsistencies.[28,53] From this data, it is clear that the VLPs improved the thermal stability of free SLDM RNAs and this could be explained by two factors: first, the proteinaceous capsid may limit transfer of water molecules or ions that are detrimental to RNA, therefore, limiting the rate of RNA degradation inside the VLPs. In fact, we have previously shown that incubation of VLPs at ambient temperature for a month retained ∼70% of the RNA cargos.[28] Without the protection by the protein shell, free SLDM RNAs are vulnerable to RNA hydrolysis. Second, SLDM RNAs packaged inside the VLPs form more condensed structures and, since the rate of RNA degradation is correlated with RNA structure, reduced RNA degradation is explained by increased RNA compactness inside the VLPs.[29,54]

Next, we assayed the stability of free SLDM RNAs and VLP-encapsidated SDLM RNAs by challenging the samples to RNase A digests at 37 °C for 30 min. As expected, free SLDM RNAs were susceptible to RNase degradation and the RNA was lost after RNase A treatment (Figure 4B, lane 3). When incubated under the same conditions but without the addition of RNase A, the SLDM RNAs remained intact, as shown by the RNA band at ∼800 nt (Figure 4B, lane 1 fresh SDLM RNAs *vs* lane 2 SDLM RNAs incubated at 37 °C for 30 min). In stark contrast, packaging the SDLM RNA into VLPs protected the nucleic acid cargo from enzymatic degradation (Figure 4B, lanes 5, 7, 9). This is consistent with previous reports highlighting that VLPs protect their RNA cargos from nuclease degradation.[29,30,41,55] Together this data highlights the benefits of encapsidating naked/free RNA into VLPs. Packing of the SDLM RNAs into VLPs conferred higher thermal stability and rendered the cargo resistant to nuclease attack.

Validation of the VLP-Based SLDM Positive Controls. Serial dilutions of total nucleic acids extracted from Qβ 1P-C19L and CCMV-C19L VLPs were validated using RT-qPCR and RT-LAMP to detect SLDM RNA (Figure 5). Given the presence of carrier RNA in the extracts, the detection of the N and RP regions by RT-LAMP required the presence of at least 4.5×10^{-14} g of total nucleic acids. Validation of the Qβ 2P-C19L VLPs required a 10-fold higher quantity of total nucleic acids (∼4.5×10^{-13} g) due to the lower quantity of encapsidated SLDM per particle. The RT-LAMP detection limit for the N and RP regions corresponded to RT-qPCR C_q values of ∼36 and ∼27, respectively. This was similar to our results obtained from the *in vitro* transcribed SLDM RNAs (see Figure 2).

Swab-to-Test RT-LAMP Assay. The swab-to-test assay allows the direct testing of samples without RNA extraction, thus reducing the need for laboratory reagents and consumables. Heating clinical samples to 95 °C for 5 min has been shown to release sufficient RNA for analysis.[24,56,57] We therefore adopted a similar strategy to test our VLP-based SLDM positive controls for RNA isolation. Indeed, RNA is released more efficiently from VLPs by thermal lysis than treatment with a commercial extraction kit.[58−60]

We analyzed the VLPs by native agarose gel electrophoresis before (t = 0 min) and after (t = 5 min) heating the particles to

https://dx.doi.org/10.1021/acs.biomac.0c01727
Biomacromolecules 2021, 22, 1231−1243

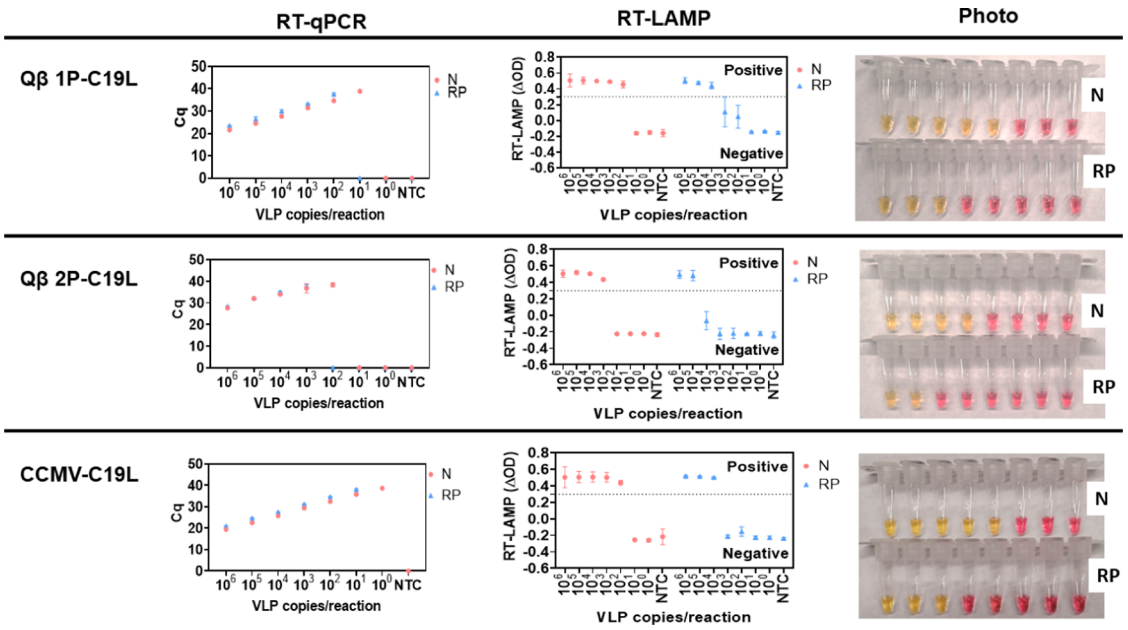

Figure 7. Serial dilutions of VLPs heated to 95 °C for 5 min to release encapsidated RNAs. The total RNA was analyzed by RT-qPCR and RT-LAMP to detect the presence of SLDM RNA. Error bars depict standard deviations. In the RT-LAMP assay, the dotted line at 0.3 on the *y*-axis separates the positive and negative clusters. Images indicate the color change in the RT-LAMP assay and are arranged according to the *x*-axis in the RT-qPCR panel (NTC = no template control).

95 °C. The RNA and protein bands were coincident at $t = 0$, but separate RNA and protein bands were observed at $t = 5$, confirming the release of RNA from the particles (Figure 6). The RNA bands at both time points were excised from the gels for analysis by RT-qPCR and RT-LAMP, revealing the presence of SLDM RNAs at both time points for all three VLP formats. The quantity of RNA released from the VLPs was similar to the quantity present in the intact particles, suggesting that heating to 95 °C releases RNA efficiently and completely.

Next, we determined the minimum VLP copy number required for the swab-to-test assay combined with RT-qPCR and RT-LAMP as detection methods (Figure 7). A minimum of 10 copies of CCMV-C19L was required to detect the N and RP regions by RT-qPCR, whereas 100 copies of Qβ 1P-C19L and 1000 copies of Qβ 2P-C19L were required due to the lower number of SLDM RNAs encapsidated in these particles. At least 10^4 CCMV-C19L and Qβ 1P-C19L VLPs were required to release sufficient SLDM RNA for the detection of both the N and RP regions by RT-LAMP due to the lower sensitivity of this method compared to RT-qPCR. Qβ 2P-C19L particles contained the lowest number of SLDM RNA molecules, and 10^5 VLPs were therefore required to detect both the N and RP regions. A minimum of 10^5 VLPs is therefore required for the successful detection of both the N and RP regions in a swab-to-test assay with the proposed primer sets and SLDM RNA, equating to 0.45 pg of Qβ 1P-C19L or Qβ 2P-C19L and 0.65 pg of CCMV-C19 for each assay. The RT-LAMP detection limit for the N and RP regions corresponded to RT-qPCR C_q values of ~35 and ~29, respectively. These observations are congruent with the findings reported above (Figures 2 and 5).

Validation of VLP-Based SLDM Positive Controls in a Clinical Setting. Finally, we used ddPCR to tabulate the absolute SLDM copy number extracted from positive controls alongside clinical samples from a COVID-19 patient and a healthy patient. All SLDM positive controls yielded amplitude signals of 3000−5000 for the N region and 5000−10 000 for the RP region (Figure 8A). The N and RP regions were detected in the COVID-19 sample, confirming their suitability as RT-qPCR targets and for the validation of the RT-LAMP assay.

CCMV-C19L contained the highest SLDM copy number (1700/μL), followed by Qβ 1P-C19L (1500−1700/μL) and Qβ 2P-C19L (<1000/μL) based on the average copy number of both N and RP (Figure 8B). Each microgram of CCMV-C19L particles therefore yielded ~5.02×10^9 SLDM molecules compared to 4.46×10^9 for Qβ 1P-C19L and 2.20×10^9 for Qβ 2P-C19L (Figure 8C). These results are congruent with our RT-qPCR data showing that CCMV-C19L encapsidated the most SLDM RNAs and that the Qβ one-plasmid system encapsidated ~50% more SLDM RNAs than the two-plasmid system (Table 1). Similar results were obtained for the encapsidation of SARS-CoV-2 Detection Module RNAs.[28]

We also validated our SLDM positive controls for the swab-to-test assay in a clinical setting. All positive controls were readily detected (above the detection limit of 0.3) together with the sample from the COVID-19 patient, with an apparent viral load of ~10^5 copies/μL (Figure 7D). This suggests our positive controls are reliable for direct RT-LAMP assays in which RNA extraction is rendered unnecessary by heating the samples to 95 °C. The color change in the RT-LAMP assay was clearly detected by the naked eye (Figure 8E).

CONCLUSIONS

We have shown that Qβ and CCMV VLPs encapsidating designer RNAs can be used as full-process positive controls in molecular assays for the detection of SARS-CoV-2. The RNAs can be extracted from the VLPs alongside clinical samples using routine methods. We tested three different VLP formats and found that CCMV-C19L particles accommodated the largest quantity of SLDM RNAs (5.02×10^9 copies) followed

https://dx.doi.org/10.1021/acs.biomac.0c01727
Biomacromolecules 2021, 22, 1231−1243

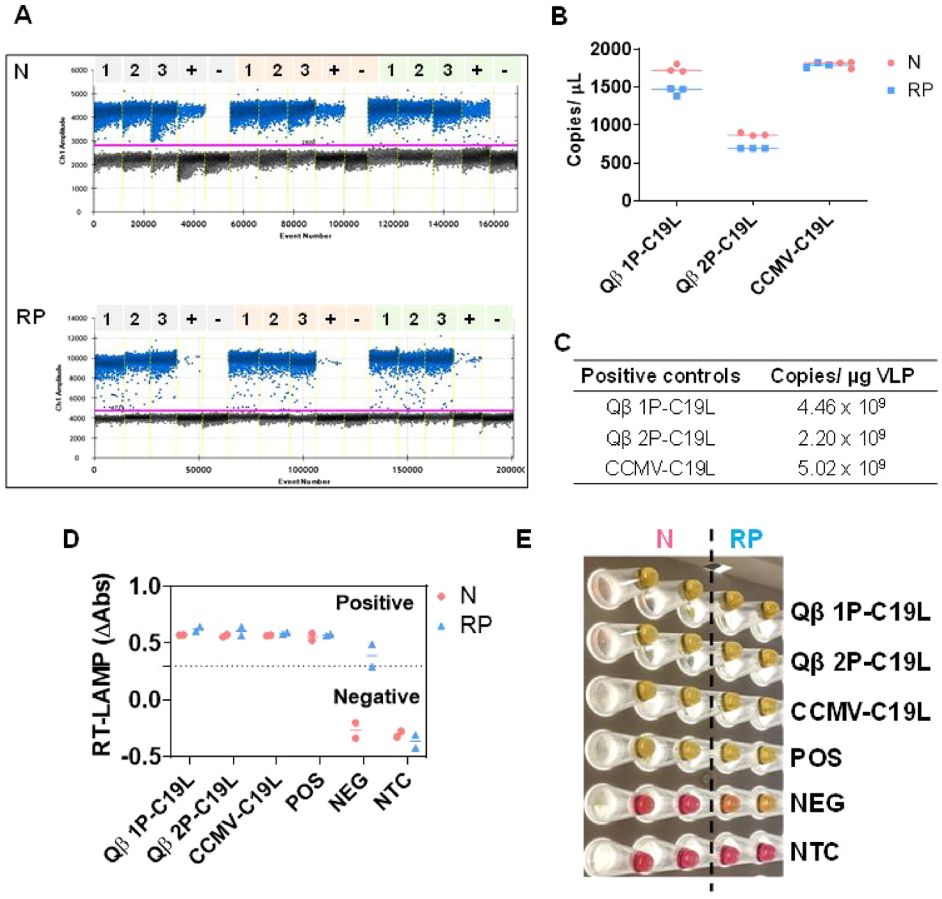

Figure 8. Validation of SLDM positive controls in clinical settings. (A) Droplet digital PCR one-dimensional amplitude plots of SARS-CoV-2 positive controls (N and RP regions): lane 1 = Qβ 1P-C19L; lane 2 = Qβ 2P-C19L; lane 3 = CCMV-C19L; lane (+) = COVID-19 patient sample; lane 5 (N) = healthy patient sample (negative control for N); and lane 5 (RP) = no template control (negative control for RP). Data represent triplicate amplifications. The pink line is the cutoff between positive clusters (blue dots) and negative clusters (black dots). (B) Scatter plot comparing N and RP copy numbers for all positive controls. The bars indicate median values. (C) SLDM RNA copy numbers detected for every microgram of SARS-CoV-2 positive controls. (D) Swab-to-test assay of SLDM positive controls with clinical samples in duplicate. The dotted line at 0.3 on the *y*-axis separates the positive and negative clusters (POS = COVID-19 patient sample, NEG = healthy patient sample, NTC = no template control). The bars indicate median values. (E) Image of the swab-to-test reaction showing the color change from pink (negative) to yellow (positive).

by Qβ 1P-C19L (4.46×10^9) and Qβ 2P-C19L (2.20×10^9). Due to the presence of carrier RNA in the recommended extraction kit, a minimum of 10^{-13} g total nucleic acids was required to detect both the N and RP regions in RT-LAMP assays. We also showed that the RP detection region could function as both an external and an internal positive control, a standard that is absent in many publications thus far. The proposed RP binding region (human *POP7* gene) is an ideal target for both RT-LAMP and RT-PCR assays. Our VLP-based SLDM positive controls were not only suitable as positive controls in standard RT-LAMP assays but also in swab-to-test assays in which samples are heated to circumvent the RNA extraction step. Heat resulted in the denaturation and disassembly of the VLPs, releasing the cargo RNAs into solution. A minimum of 10^5 copies of VLPs was required for optimal performance as a positive control in the swab-to-test assay. Our VLP-based controls increase thermal stability and protect the RNA cargoes from enzymatic degradation. The VLPs are therefore suitable as positive controls for RT-LAMP point-of-care diagnostic systems as well as at-home test kits to achieve reliable and scalable mass testing.

■ ASSOCIATED CONTENT

Supporting Information

The Supporting Information is available free of charge at https://pubs.acs.org/doi/10.1021/acs.biomac.0c01727.

Maps of the plasmids used for the production; construction of the SARS-CoV-2 LAMP detection module (SLDM); characterization of *in vitro* transcribed SLDM RNA; batch-to-batch consistency of the SLDM-loaded VLPs; primers and oligonucleotides used to construct the SLDM, (PDF)

■ AUTHOR INFORMATION

Corresponding Author

Nicole F. Steinmetz − *Department of NanoEngineering, Department of Radiology, Department of Bioengineering, Center for Nano-ImmunoEngineering, Moores Cancer Center, and Institute for Materials Discovery and Design, University of California−San Diego, La Jolla, California 92093, United States;* orcid.org/0000-0002-0130-0481; Email: nsteinmetz@ucsd.edu

https://dx.doi.org/10.1021/acs.biomac.0c01727
Biomacromolecules 2021, 22, 1231−1243

Authors

Soo Khim Chan − *Department of NanoEngineering, University of California−San Diego, La Jolla, California 92093, United States*

Pinyi Du − *Department of Medicine, University of California−San Diego, La Jolla, California 92093, United States*

Caroline Ignacio − *Department of Medicine and Veterans Administration San Diego Healthcare System, University of California−San Diego, La Jolla, California 92093, United States*

Sanjay Mehta − *Department of Medicine, University of California−San Diego, La Jolla, California 92093, United States*

Isabel G. Newton − *Department of Radiology and Veterans Administration San Diego Healthcare System, University of California−San Diego, La Jolla, California 92093, United States*

Complete contact information is available at: https://pubs.acs.org/10.1021/acs.biomac.0c01727

Author Contributions

S.K.C. designed the VLPs and performed the experimental work. P.D. and C.I. performed assays on patient samples. S.M. and I.G.N. helped with the project development. N.F.S. conceived the study and oversaw the VLP design and testing. S.K.C. and N.F.S. wrote the manuscript. All authors read and edited the manuscript.

Notes

The authors declare no competing financial interest.

■ ACKNOWLEDGMENTS

This work was funded in part by grants from the National Science Foundation: RAPID CBET-2032196 and RAPID CMMI-2027668, as well as the University of California: UCOP-R00RG2471 and a Galvanizing Engineering in Medicine (GEM) Award. We thank Drs. Vero Beiss and Oscar Ortega-Rivera (UC San Diego) for helpful discussion regarding VLP design.

■ REFERENCES

(1) COVID-19 Map - Johns Hopkins Coronavirus Resource Center. https://coronavirus.jhu.edu/map.html (accessed Nov 15 , 2020).

(2) Pokhrel, P.; Hu, C.; Mao, H. Detecting the Coronavirus (COVID-19). *ACS Sens.* **2020**, *5*, 2283−2296.

(3) Testing Data in the U.S. https://www.cdc.gov/coronavirus/2019-ncov/cases-updates/testing-in-us.html (accessed Aug 8 , 2020).

(4) Udugama, B.; Kadhiresan, P.; Kozlowski, H. N.; Malekjahani, A.; Osborne, M.; Li, V. Y. C.; Chen, H.; Mubareka, S.; Gubbay, J. B.; Chan, W. C. W. Diagnosing COVID-19: The Disease and Tools for Detection. *ACS Nano* **2020**, *14*, 3822−3835.

(5) Carter, L. J.; Garner, L. V.; Smoot, J. W.; Li, Y.; Zhou, Q.; Saveson, C. J.; Sasso, J. M.; Gregg, A. C.; Soares, D. J.; Beskid, T. R.; et al. Assay Techniques and Test Development for COVID-19 Diagnosis. *ACS Cent. Sci.* **2020**, *6*, 591−605.

(6) Guglielmi, G. The Explosion of New Coronavirus Tests That Could Help to End the Pandemic. *Nature* **2020**, *583*, 506−509.

(7) Emergency Use Authorization (EUA) Summary for the COLOR SARS-CoV-2 LAMP Diagnostic Assay. https://www.fda.gov/media/138249/download (accessed Aug 10 , 2020).

(8) Abbott RealTime SARS-CoV-2. https://www.fda.gov/media/136258/download (accessed Aug 10 , 2020).

(9) First Point-of-Care Test for COVID-19 Leveraging CRISPR Technology. https://www.genengnews.com/virology/coronavirus/first-point-of-care-test-for-covid-19-leveraging-crispr-technology/ (accessed Aug 10 , 2020).

(10) Hooper, M. W.; Nápoles, A. M.; Pérez-Stable, E. J. COVID-19 and Racial/Ethnic Disparities. *Jama* **2020**, *323*, 2466−2467.

(11) AQ-TOPTM COVID-19 Rapid Detection Kit. https://www.fda.gov/media/138307/download (accessed Aug 18 , 2020).

(12) Larremore, D. B.; Wilder, B.; Lester, E.; Shehata, S.; Burke, J. M.; Hay, J. A.; Tambe, M.; Mina, M. J.; Parker, R. Test Sensitivity Is Secondary to Frequency and Turnaround Time for COVID-19 Surveillance. *Sci. Adv.* **2020**, *7*, No. eabd5393.

(13) Ahn, S. J.; Baek, Y. H.; Lloren, K. K. S.; Choi, W. S.; Jeong, J. H.; Antigua, K. J. C.; Kwon, H. Il.; Park, S. J.; Kim, E. H.; Kim, Y. Il.; Si, Y. J.; Hong, S. B.; Shin, K. S.; Chun, S.; Choi, Y. K.; Song, M. S. Rapid and Simple Colorimetric Detection of Multiple Influenza Viruses Infecting Humans Using a Reverse Transcriptional Loop-Mediated Isothermal Amplification (RT-LAMP) Diagnostic Platform. *BMC Infect. Dis.* **2019**, *19*, No. 676.

(14) Oloniniyi, O. K.; Kurosaki, Y.; Miyamoto, H.; Takada, A.; Yasuda, J. Rapid Detection of All Known Ebolavirus Species by Reverse Transcription-Loop-Mediated Isothermal Amplification (RT-LAMP). *J. Virol. Methods* **2017**, *246*, 8−14.

(15) da Silva, S. J. R.; Paiva, M. H. S.; Guedes, D. R. D.; Krokovsky, L.; de Melo, F. L.; da Silva, M. A. L.; da Silva, A.; Ayres, C. F. J.; Pena, L. J. Development and Validation of Reverse Transcription Loop-Mediated Isothermal Amplification (RT-LAMP) for Rapid Detection of ZIKV in Mosquito Samples from Brazil. *Sci. Rep.* **2019**, *9*, No. 4494.

(16) Yan, C.; Cui, J.; Huang, L.; Du, B.; Chen, L.; Xue, G.; Li, S.; Zhang, W.; Zhao, L.; Sun, Y.; Yao, H.; Li, N.; Zhao, H.; Feng, Y.; Liu, S.; Zhang, Q.; Liu, D.; Yuan, J. Rapid and Visual Detection of 2019 Novel Coronavirus (SARS-CoV-2) by A Reverse Transcription Loop-Mediated Isothermal Amplification Assay. *Clin. Microbiol. Infect.* **2020**, *26*, 773−779.

(17) Lamb, L. E.; Bartolone, S. N.; Ward, E.; Chancellor, M. B. Chancellor, M. B. Rapid Detection of Novel Coronavirus/Severe Acute Respiratory Syndrome Coronavirus 2 (SARS-CoV-2) by Reverse Transcription-Loop-Mediated Isothermal Amplification. *PLoS One* **2020**, *15*, No. e0234682.

(18) Baek, Y. H.; Um, J.; Antigua, K. J. C.; Park, J. H.; Kim, Y.; Oh, S.; Kim, Y. il.; Choi, W. S.; Kim, S. G.; Jeong, J. H.; Chin, B. S.; Nicolas, H. D. G.; Ahn, J. Y.; Shin, K. S.; Choi, Y. K.; Park, J. S.; Song, M. S. Development of a Reverse Transcription-Loop-Mediated Isothermal Amplification as a Rapid Early-Detection Method for Novel SARS-CoV-2. *Emerging Microbes Infect.* **2020**, *9*, 998−1007.

(19) Notomi, T.; Okayama, H.; Masubuchi, H.; Yonekawa, T.; Watanabe, K.; Amino, N.; Hase, T. Loop-Mediated Isothermal Amplification of DNA. *Nucleic Acids Res.* **2000**, *28*, No. e63.

(20) Harper, S. J.; Ward, L. I.; Clover, G. R. G. Development of LAMP and Real-Time PCR Methods for the Rapid Detection of Xylella Fastidiosa for Quarantine and Field Applications. *Phytopathology* **2010**, *100*, 1282−1288.

(21) Zhu, X.; Wang, X.; Han, L.; Chen, T.; Wang, L.; Li, H.; Li, S.; He, L.; Fu, X.; Chen, S.; Xing, M.; Chen, H.; Wang, Y. Multiplex Reverse Transcription Loop-Mediated Isothermal Amplification Combined with Nanoparticle-Based Lateral Flow Biosensor for the Diagnosis of COVID-19. *Biosens. Bioelectron.* **2020**, *166*, No. 112437.

(22) Zhang, Y.; Tanner, N. A. Development of Multiplexed RT-LAMP for Detection of SARS-CoV-2 and Influenza Viral RNA Doi: MedRxiv Preprint. *medRxiv* **2020**, DOI: 10.26/20219972d.

(23) Lion, T. Current Recommendations for Positive Controls in RT-PCR Assays. *Leukemia* **2001**, *15*, 1033−1037.

(24) Dao Thi, V. L.; Herbst, K.; Boerner, K.; Meurer, M.; Kremer, L. P.; Kirrmaier, D.; Freistaedter, A.; Papagiannidis, iD.; Galmozzi, C.; Stanifer, M. L.; Boulant, S.; Klein, S.; Chlanda, P.; Khalid, D.; Miranda, I. B.; Schnitzler, P.; Kräusslich, H.-G.; Knop, M.; Anders, S. A Colorimetric RT-LAMP Assay and LAMP-Sequencing for Detecting SARS-CoV-2 RNA in Clinical Samples. *Sci. Transl. Med.* **2020**, *12*, No. eabc7075.

(25) Kitagawa, Y.; Orihara, Y.; Kawamura, R.; Imai, K.; Sakai, J.; Tarumoto, N.; Matsuoka, M.; Takeuchi, S.; Maesaki, S.; Maeda, T. Evaluation of Rapid Diagnosis of Novel Coronavirus Disease (COVID-19) Using Loop-Mediated Isothermal Amplification. *J. Clin. Virol.* **2020**, *129*, No. 104446.
(26) Huang, W. E.; Lim, B.; Hsu, C.; Xiong, D.; Wu, W.; Yu, Y.; Jia, H.; Wang, Y.; Zeng, Y.; Ji, M.; Chang, H.; Zhang, X.; Wang, H.; Cui, Z. RT-LAMP for Rapid Diagnosis of Coronavirus SARS-CoV-2. *Microb. Biotechnol.* **2020**, *13*, 950−961.
(27) MobileDetect-BIO BCC19 Test Kit - Instructions for Use. https://www.fda.gov/media/141791/download (accessed Nov 15 , 2020).
(28) Chan, S. K.; Du, P.; Ignacio, C.; Mehta, S.; Newton, I. G.; Steinmetz, N. F. Biomimetic Virus-Like Particles as Severe Acute Respiratory Syndrome Coronavirus 2 Diagnostic Tools. *ACS Nano* **2020**, *15*, 1259−1272.
(29) Fang, P.-Y.; Bowman, J. C.; Ramos, L. M. G.; Hsiao, C.; Williams, L. D. RNA: Packaged and Protected by VLPs. *RSC Adv.* **2018**, *8*, 21399−21406.
(30) Biddlecome, A.; Habte, H. H.; McGrath, K. M.; Sambanthamoorthy, S.; Wurm, M.; Sykora, M. M.; Knobler, C. M.; Lorenz, I. C.; Lasaro, M.; Elbers, K.; Gelbart, W. M. Delivery of Self-Amplifying RNA Vaccines in in Vitro Reconstituted Virus-Like Particles. *PLoS One* **2019**, *14*, No. e0215031.
(31) Chung, Y. H.; Cai, H.; Steinmetz, N. F. Viral Nanoparticles for Drug Delivery, Imaging, Immunotherapy, and Theranostic Applications. *Adv. Drug Delivery Rev.* **2020**, *156*, 214−235.
(32) Barba, A. A.; Bochicchio, S.; Dalmoro, A.; Lamberti, G. Lipid Delivery Systems for Nucleic-Acid-Based-Drugs: From Production to Clinical Applications. *Pharmaceutics* **2019**, *11*, No. 360.
(33) Raval, N.; Jogi, H.; Gondaliya, P.; Kalia, K.; Tekade, R. K. Method and Its Composition for Encapsulation, Stabilization, and Delivery of SiRNA in Anionic Polymeric Nanoplex: An In Vitro- In Vivo Assessment. *Sci. Rep.* **2019**, *9*, No. 16047.
(34) Tanner, N. A.; Zhang, Y.; Evans, T. C. Visual Detection of Isothermal Nucleic Acid Amplification Using PH-Sensitive Dyes. *Biotechniques* **2015**, *58*, 59−68.
(35) Bancroft, J. B. The Self-Assembly of Spherical Plant Viruses. In *Advances in Virus Research*; Maramorosch, K. S.; Max, A. L.; Frederik, B. B., Eds.; Academic Press: New York, 1970; Vol. *16*, pp 99−134.
(36) Cadena-Nava, R. D.; Comas-Garcia, M.; Garmann, R. F.; Rao, A. L. N.; Knobler, C. M.; Gelbart, W. M. Self-Assembly of Viral Capsid Protein and RNA Molecules of Different Sizes: Requirement for a Specific High Protein/RNA Mass Ratio. *J Virol.* **2012**, *86*, 3318−3326.
(37) Annamalai, P.; Rao, A. L. N. Dispensability of 3′ TRNA-Like Sequence for Packaging Cowpea Chlorotic Mottle Virus Genomic RNAs. *Virology* **2005**, *332*, 650−658.
(38) Witherell, G. W.; Uhlenbeck, O. C. Specific RNA Binding by Q. Beta. Coat Protein. *Biochemistry* **1989**, *28*, 71−76.
(39) Fang, P.-Y.; Gómez Ramos, L. M.; Holguin, S. Y.; Hsiao, C.; Bowman, J. C.; Yang, H.-W.; Williams, L. D. Functional RNAs: Combined Assembly and Packaging in VLPs. *Nucleic Acids Res.* **2017**, *45*, 3519−3527.
(40) Herbert, F. C.; Brohlin, O. R.; Galbraith, T.; Benjamin, C.; Reyes, C. A.; Luzuriaga, M. A.; Shahrivarkevishahi, A.; Gassensmith, J. J. Supramolecular Encapsulation of Small-Ultrared Fluorescent Proteins in Virus-Like Nanoparticles for Noninvasive in Vivo Imaging Agents. *Bioconjugate Chem.* **2020**, *31*, 1529−1536.
(41) Comas-Garcia, M.; Cadena-Nava, R. D.; Rao, A. L. N.; Knobler, C. M.; Gelbart, W. M. In Vitro Quantification of the Relative Packaging Efficiencies of Single-Stranded RNA Molecules by Viral Capsid Protein. *J. Virol.* **2012**, *86*, 12271−12282.
(42) Asuragen Develops Armored RNA Quant SARS-CoV-2 Control https://www.biospace.com/article/releases/asuragen-develops-armored-rna-quant-sars-cov-2-control/ (accessed Jul 15 , 2020).
(43) Yao, L.; Li, F.; Qu, M.; Guo, Y.; Jiang, Y.; Wang, L.; Zhai, Y. Development and Evaluation of a Novel Armored RNA Technology Using Bacteriophage Q*β*. *Food Environ. Virol.* **2019**, *11*, 383−392.
(44) Golmohammadi, R.; Fridborg, K.; Bundule, M.; Valegård, K.; Liljas, L. The Crystal Structure of Bacteriophage Q*β* at 3.5 Å Resolution. *Structure* **1996**, *4*, 543−554.
(45) PCR - QIAGEN. https://www.qiagen.com/fi/service-and-support/learning-hub/molecular-biology-methods/pcr/ (accessed Nov 10 , 2020).
(46) Svec, D.; Tichopad, A.; Novosadova, V.; Pfaffl, M. W.; Kubista, M. How Good Is a PCR Efficiency Estimate: Recommendations for Precise and Robust QPCR Efficiency Assessments. *Biomol. Detect. Quantif.* **2015**, *3*, 9−16.
(47) Vogels, C. B. F.; Brito, A. F.; Wyllie, A. L.; Fauver, J. R.; Ott, I. M.; Kalinich, C. C.; Petrone, M. E.; Casanovas-Massana, A.; Muenker, M. C.; Moore, A. J.; et al. Analytical Sensitivity and Efficiency Comparisons of SARS-CoV-2 RT−QPCR Primer−Probe Sets. *Nat. Microbiol.* **2020**, *5*, 1299−1305.
(48) Jung, Y. J.; Park, G.-S.; Moon, J. H.; Ku, K.; Beak, S.-H.; Kim, S.; Park, E. C.; Park, D.; Lee, J.-H.; Byeon, C. W.; et al. Comparative Analysis of Primer-Probe Sets for the Laboratory Confirmation of SARS-CoV-2. *ACS Infect. Dis.* **2020**, *6*, 2513−2523.
(49) Hu, X.; Deng, Q.; Li, J.; Chen, J.; Wang, Z.; Zhang, X.; Fang, Z.; Li, H.; Zhao, Y.; Yu, P.; Li, W.; Wang, X.; Li, S.; Zhang, L.; Hou, T. Development and Clinical Application of a Rapid and Sensitive Loop-Mediated Isothermal Amplification Test for SARS-CoV-2 Infection. *mSphere* **2020**, *5*, No. e00808-20.
(50) Lau, Y. L.; Ismail, I.; Izati Mustapa, N.; Yee Lai, M.; Suhaila Tuan Soh, T.; Hassan, A.; Peariasamy, K. M.; Leng Lee, Y.; Min Chong, Y.; Sam, I.-C.; Pin Goh, P. Real-Time Reverse Transcription Loop-Mediated Isothermal Amplification for Rapid Detection of SARS-CoV-2. *PeerJ* **2020**, *8*, No. e9278.
(51) Doucet, M.; El-Turabi, A.; Zabel, F.; Hunn, B. H. M.; Bengoa-Vergniory, N.; Cioroch, M.; Ramm, M.; Smith, A. M.; Gomes, A. C.; Cabral de Miranda, G.; et al. Preclinical Development of a Vaccine against Oligomeric Alpha-Synuclein Based on Virus-Like Particles. *PLoS One* **2017**, *12*, No. e0181844.
(52) Cai, H.; Shukla, S.; Steinmetz, N. F. The Antitumor Efficacy of CpG Oligonucleotides Is Improved by Encapsulation in Plant Virus-Like Particles. *Adv. Funct. Mater.* **2020**, *30*, No. 1908743.
(53) Seelenfreund, E.; Robinson, W. A.; Amato, C. M.; Tan, A.-C.; Kim, J.; Robinson, S. E. Long Term Storage of Dry versus Frozen RNA for Next Generation Molecular Studies. *PLoS One* **2014**, *9*, No. e111827.
(54) Gopal, A.; Egecioglu, D. E.; Yoffe, A. M.; Ben-Shaul, A.; Rao, A. L. N.; Knobler, C. M.; Gelbart, W. M. Viral RNAs Are Unusually Compact. *PLoS One* **2014**, *9*, No. e105875.
(55) Zhang, L.; Sun, Y.; Chang, L.; Jia, T.; Wang, G.; Zhang, R.; Zhang, K.; Li, J. A Novel Method to Produce Armored Double-Stranded DNA by Encapsulation of MS2 Viral Capsids. *Appl. Microbiol. Biotechnol.* **2015**, *99*, 7047−7057.
(56) Smyrlaki, I.; Ekman, M.; Lentini, A.; Rufino de Sousa, N.; Papanicolaou, N.; Vondracek, M.; Aarum, J.; Safari, H.; Muradrasoli, S.; Rothfuchs, A. G.; Albert, J.; Högberg, B.; Reinius, B. Massive and Rapid COVID-19 Testing Is Feasible by Extraction-Free SARS-CoV-2 RT-PCR. *Nat. Commun.* **2020**, *11*, No. 4812.
(57) Rabe, B. A.; Cepko, C. SARS-CoV-2 Detection Using Isothermal Amplification and a Rapid, Inexpensive Protocol for Sample Inactivation and Purification. *Proc. Natl. Acad. Sci. U.S.A.* **2020**, *117*, 24450−24458.
(58) Yu, X. F.; Pan, J. C.; Ye, R.; Xiang, H. Q.; Kou, Y.; Huang, Z. C. Preparation of Armored RNA as a Control for Multiplex Real-Time Reverse Transcription-PCR Detection of Influenza Virus and Severe Acute Respiratory Syndrome Coronavirus. *J. Clin. Microbiol.* **2008**, *46*, 837−841.
(59) Crone, M. A.; Priestman, M.; Ciechonska, M.; Jensen, K.; Sharp, D. J.; Anand, A.; Randell, P.; Storch, M.; Freemont, P. S. A Role for Biofoundries in Rapid Development and Validation of

Automated SARS-CoV-2 Clinical Diagnostics. *Nat. Commun.* **2020**, *11*, No. 4464.
(60) Hasan, M. R.; Mirza, F.; Al-Hail, H.; Sundararaju, S.; Xaba, T.; Iqbal, M.; Alhussain, H.; Yassine, H. M.; Perez-Lopez, A.; Tang, P. Detection of SARS-CoV-2 RNA by Direct RT-QPCR on Nasopharyngeal Specimens without Extraction of Viral RNA. *PLoS One* **2020**, *15*, No. e0236564.

https://dx.doi.org/10.1021/acs.biomac.0c01727
Biomacromolecules 2021, 22, 1231−1243